Molecular Catalysis 509 (2021) 111636

Contents lists available at ScienceDirect

Molecular Catalysis

journal homepage: www.journals.elsevier.com/molecular-catalysis

Experimental and DFT study on titanium-based half-sandwich metallocene catalysts and their application for production of 1-hexene from ethylene

Sajjad Gharajedaghi [a], Zahra Mohamadnia [a,*], Ebrahim Ahmadi [b], Mohamadreza Marefat [b], Gerard Pareras [c,d], Sílvia Simon [c], Albert Poater [c,*], Naeimeh Bahri-Laleh [e,*]

[a] Polymer Research Laboratory, Department of Chemistry, Institute for Advanced Studies in Basic Science (IASBS), Gava Zang, Zanjan 45137-66731, Iran
[b] Polymer Research Laboratory, Department of Chemistry, Faculty of Science, University of Zanjan, Zanjan, Iran
[c] Institut de Química Computacional i Catàlisi and Departament de Química, Universitat de Girona, c/Maria Aurèlia Capmany 69, Girona, Catalonia 17003, Spain
[d] School of Chemistry, University College Cork, College Road, Cork, Ireland
[e] Polymerization Engineering Department, Iran Polymer and Petrochemical Institute (IPPI), P.O. Box 14965/115, Tehran, Iran

A B S T R A C T

Different types of [Ind-C(R)-Phenyl]$TiCl_3$ catalysts based on pendant arene containing indenyl (Ind) ligand bearing various types of bridges (R=*cyclo*-C_5H_{10} (C1), $(CH_3)_2$ (C2), 4-*t*Bu-*cyclo*-C_5H_9 (C3), and *cyclo*-C_6H_{12} (C4)) have been synthesized, and used in the ethylene trimerization to 1-hexene in the presence of methyl aluminoxane (MAO) as co-catalyst. The reaction conditions were first optimized in C2 catalyst case, where the highest 1-hexene product was achieved at the catalyst concentration, temperature and ethylene pressure of 1.5×10^{-3} M, 40 °C, and 8 bar, respectively. During this optimization and under specific reaction conditions, a switching behavior from ethylene trimerization to polymerization was also detected, as an undesired reaction. At the optimized conditions, synthesized catalysts showed the following trend toward both 1-hexene yield and selectivity: C1>C2>C3>C4. Then, to shed light on the possible reaction mechanisms and to confirm the activity trend obtained in experimental section, density functional theory (DFT) calculations were employed. In this line, obtained results for activity trend in the simulation studies fit well with the experiments. According to both experimental and DFT results, the highest catalytic activity was observed in the presence of the catalyst with a cyclohexane middle bridge (C1).

Introduction

The oligomerization of linear terminal alkenes is one of the significant problems in the linear α-olefins (LAOs) production in both industry and academia [1–6], together with hydrogenation of alkanes [7]. Linear alpha olefins, normally produced by ethylene oligomerization processes [8–11], and by Fischer–Tropsch synthesis followed by purification [12], found applications as co-monomers in high density and linear low density polyethylene (HDPE and LLDPE) production, and as detergents, plasticizers, surfactants, and lubricants.[13,14]. Traditional technology for LAO synthesis is based on a full-range production process in which ethylene oligomerizes to achieve a broad range of the products. It is a non-selective approach and cannot match the constantly growing market demand. Accordingly, the change of a statistical ethylene oligomerization process into selective approach appears highly demanded [13–15]. The selective oligomerization of ethylene has recently attracted considerable attention [16,17]. In this regard, the catalytically selective trimerization of ethylene to 1-hexene has been extensively studied [18–23]. Amongst all the systems, the catalysts based on chromium metal has attracted more attention in the recent years [23,24]. This metal is the main center of Phillips' Cr-pyrrolide catalysts [25]. BP's (*o*-OMe)PNP catalysts [26], Sasol's PNP/SNS trimerization catalysts [27,28], and PNP tetramerization catalysts [29]. Catalysts based on other transition metals such as Zr, Ti, V, Ta, or Ni have been less studied [30,31].

Hessen's group in 2001 for the first time reported that the change of R from methyl to phenyl in [(η^5-$C_5H_4C(Me)_2RTiCl_3$]/MAO, switches the reaction from ethylene polymerization into ethylene trimerization and facilitates formation of 1-hexene as the major product. The hemilabile behavior of cyclopentadienyl ligand with the arene group is the main reason of this significant change in catalyst behavior [32]. Deckers et al. in 2002 synthesized a new family of highly active catalysts for the trimerization of ethylene based on (arene-cyclopentadienyl) titanium complexes [(η^5-C_5H_3R-(bridge)-$ArTiCl_3$] activated by MAO co-catalyst. Selectivity to produce 1-hexene not only depends on the presence of the arene pendant group but also the bridge nature between cyclopentadienyl (Cp) and arene. In the absence of arene, polyethylene was the main product [33,34]. Huang's group synthesized a half-sandwich

* Corresponding authors.
E-mail addresses: z.mohamadnia@iasbs.ac.ir (Z. Mohamadnia), albert.poater@udg.edu (A. Poater), n.bahri@ippi.ac.ir (N. Bahri-Laleh).

https://doi.org/10.1016/j.mcat.2021.111636
Received 3 April 2021; Received in revised form 7 May 2021; Accepted 8 May 2021
Available online 28 May 2021

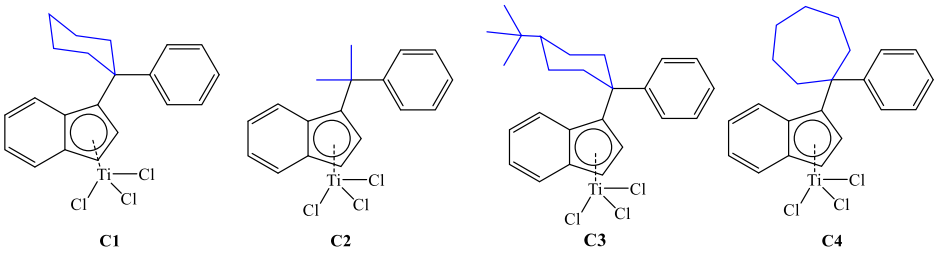

Scheme 1. Titanium-based catalysts C1–C4 (in blue the bridge).

titanium complex containing pendant thienyl group and used it in ethylene trimerization. In the reported results, they affirmed the important role of thiophene in ethylene trimerization [35]. Cp-based ligands have been widely studied as important ligands in organometallic chemistry and most studies on Cp modification can be focused on the type of the bearing pendant group on it. In this regard, in 2004, Huang et al. used half-sandwich titanium complexes with the pendant ethereal group activated by MAO for ethylene trimerization [36]. In 2013, Zhang et al. synthesized half-sandwich indenyl-based titanium complexes [Ind-(bridge)-Ar]$TiCl_3$ bearing pendant arene group on the indenyl ring and examined the selective ethylene trimerization in the presence of MAO co-catalyst [37–39]. In the following of previous works, Zhang et al. synthesized another series of half-sandwich indenyl-based titanium complexes with the thienyl group (Cp(Ind)-bridge--thienyl]$TiCl_3$, which showed high selectivity in ethylene trimerization and its conversion to 1-hexene [23]. In 2015, Varga et al. synthesized and characterized two titanium-based heterogeneous catalysts using different methods including grafting through a covalent Ti-O-Si bond as well as through a pendant flexible tether from the Cp ligand [40]. The catalyst synthesized by the second method did not show any activity in ethylene trimerization because the active species were too close to the support surface [40]. In 2015, Duchateau et al. synthesized different types of phenoxy-imine titanium catalyst according to the Fujita method and examined homogeneous and heterogeneous types [41]. Despite the high activity and selectivity of the synthesized titanium catalysts, very little polyethylene was produced as a by-product. In this work, an attempt was also made to stabilize the catalyst and prevent the formation of the polymer, while maintaining the desired catalyst activity and selectivity. In this line, MAO co-catalyst and phenoxy-imine titanium catalysts were stabilized using a two-step process on silica carrier [41]. In 2019, Mohamadnia et al. successfully synthesized and identified three titanium-based catalysts {[η^5-C_9H_6-C(R)]-C_4H_3S}$TiCl_3$ with different bridges (cyclohexane, cyclopentane and dimethyl) active in ethylene trimerization [29]. Factors affecting the catalyst activity in the production of 1-hexene including catalyst concentration, ethylene pressure, and reaction temperature were optimized [29].

In the following of our research on the selective trimerization of ethylene, due to the high importance of α-olefins in the petrochemical industry, here a series of indenyl half-sandwich titanium complexes, namely [Ind-C(R)-phenyl]$TiCl_3$ was synthesized for possible application in ethylene trimerization process. The main aim is to fulfill the process at mild operating conditions such as low pressure and temperature to reduce operator-related risks, and to reach high economic efficiency by reducing catalyst consumption. In this regard, the effect of the arene bridge and indenyl ring, temperature, ethylene pressure, and MAO and catalyst concentrations on the catalytic efficiency was investigated. Furthermore, the effect of ligand type on the 1-hexene selectivity was also examined using DFT simulations by considering the energy path for each catalyst (C1-C4, see Scheme 1), during ethylene oligomerization process [42–44].

Experimental

Materials

All manipulations of water- and/or air-sensitive compounds were performed using standard Schlenk and glove-box techniques under deoxygenated argon or nitrogen. The modified MAO (MMAO) co-

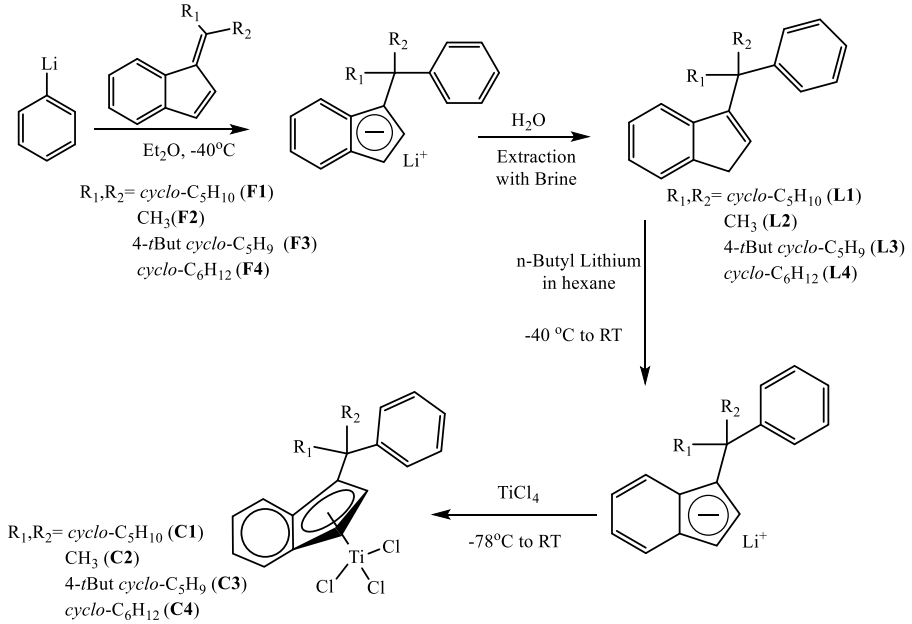

Scheme 2. General procedure for synthesis of benzofulvene precursors, ligands and corresponding titanium-based catalysts.

catalyst (7 wt% in toluene), titanium tetrachloride ($TiCl_4$), n-butyllithium (n-BuLi; 2.5 M in n-hexane), phenyllithium (1.5 M in dibutyl ether), and molecular sieve were obtained from Aldrich (Germany). Indene, pyrrolidine, 4-tert-butylcyclohexanone, cyclohexanone, cycloheptanone, acetone, ethanol, n-hexane, diethyl ether, toluene, Na_2CO_3, $MgSO_4$, NaCl, Na_2SO_4, sodium, and NaOH were purchased from Merck (Germany). Ethylene was provided by Bandar Imam Petrochemical Company (Iran) and purified by passing through NaOH, activated silica gel, and molecular sieve (3 Å) columns, respectively. Methanol, n-hexane, toluene and diethyl ether were dried and vacuum-distilled using calcium hydride (CaH_2) and sodium metal consecutively before use.

Characterization of ligands, catalysts, trimerization products

The ^{1}H NMR and ^{13}C NMR spectra have been recorded by the Bruker 400 MHz Ultra shield NMR instrument (Germany) at room temperature. The progress of the catalyst synthesis and trimerization reactions was followed by thin-layer chromatography (TLC) and gas chromatography GC system (Varian CP 3800), respectively. The inductively coupled plasma analysis (ICP), model 3410 ARL made in Switzerland, was used to determine the metal components of the catalyst. The UV-visible spectrophotometer (Pharmacia Biotech Ultrospec 4000) was used to further examine the spectral characteristics of synthetic complexes. Elemental analysis was performed using a Vario EL III CHNS elemental analyzer.

General procedure for the synthesis of benzofulvene precursors C_9H_6-C(R) (R=cyclo-C_5H_{10} (F1), $(CH_3)_2$ (F2), 4-tBu-cyclo-C_5H_9 (F3), cyclo-C_6H_{12} (F4))

The different fulvene precursors F1–F4 were synthesized with a slight change according to the method proposed by Stone and Little (Scheme 2) [45]. For this purpose, freshly distilled indene (5 mmol, 0.58 mL) and freshly distilled pyrrolidine (3 mmol, 0.25 mL) were dissolved in 2 mL of methanol under argon atmosphere at ambient temperature. Then, different ketones)2 mmol(, such as cyclohexanone, cycloheptanone, 4-*t*-butyl cyclohexanone, and acetone, were added dropwise to the stirred solution and the reaction mixture was stirred for 12 h. At the end of the reaction, acetic acid (3 mmol, 0.18 mL) was added to neutralize the residual base, and dilution was performed with diethyl ether (10 mL). To separate the remaining indene, and other unreacted materials, extraction was performed with deionized water (3 × 10 mL) followed by brine (2 × 10 mL). Finally, the water remaining in the organic phase was dried by anhydrous $MgSO_4$. Synthesized fulvenes were purified using column chromatography by silica gel (petroleum ether as eluent). The pure fulvenes were characterized using ^{1}H NMR, ^{13}C NMR, and FT-IR spectroscopies.

Characterization of C_9H_6-C(cyclo-C_5H_{10}) (F1)

Fulvene ($C_{15}H_{16}$, F1) was obtained as white crystals in 70% yield. ^{1}H NMR (400 MHz, $CDCl_3$, δ, ppm): 1.70–1.79 (2H, m, C_9H_6-C(*cyclo*-C_5H_{10})), 1.79–1.9 (4H, m, C_9H_6-C(*cyclo*-C_5H_{10})), 2.75 (2H, t, C_9H_6-C(*cyclo*-C_5H_{10})), 3.05 (2H, t, C_9H_6-C(*cyclo*-C_5H_{10})), 6.79 (1H, d, C_9H_6-C(*cyclo*-C_5H_{10})), 6.94 (1H, d, C_9H_6-C(*cyclo*-C_5H_{10})), 7.17–7.27 (2H, m, C_9H_6-C(*cyclo*-C_5H_{10})), 7.37 (1H, d, C_9H_6-C(*cyclo*-C_5H_{10})), 7.9 (1H, d, C_9H_6-C(*cyclo*-C_5H_{10})). ^{13}C NMR (100 MHz, $CDCl_3$, δ, ppm): 26.40, 28.10, 28.76, 32.29, 34.48 (*C*H_2), 121.05, 123.73, 124.64, 126.01, 127.30, 128.25 (*C*H), 133.65, 135.87, 144.56, 152.46 (*C*$_q$). FT-IR (KBr, υ_{max}, cm^{-1}): 3010, 3014 and 3064 (sp^2 C-H), 2848 and 2921 (sp^3 C-H), 1780–1930 (overtone of aromatic ring), 1619 (C=C), 1443 (CH_2), 723 and 740 (=C-H) (Figs. S1–S3).

Characterization of C_9H_6-C$(CH_3)_2$ (F2)

Fulvene ($C_{12}H_{12}$, F2) was obtained as a yellow oil in 70% yield. ^{1}H NMR (400 MHz, $CDCl_3$, δ, ppm): 2.31 (3H, s, C_9H_6-C(CH_3)$_2$), 2.54 (3H, s, C_9H_6-C(CH_3)$_2$), 6.84 (1H, d, C_9H_6-C$(CH_3)_2$), 6.91 (1H, d, C_9H_6-C$(CH_3)_2$), 7.25–7.32 (2H, m, C_9H_6-C$(CH_3)_2$), 7.41 (1H, d, C_9H_6-C$(CH_3)_2$), 7.82 (1H, d, C_9H_6-C$(CH_3)_2$). ^{13}C NMR (100 MHz, $CDCl_3$, δ, ppm): 22.84, 25.00 (*C*H_3), 121.03, 123.52, 124.71, 126.02, 127.61, 128.35 (*C*H), 135.74, 136.70, 143.38, 143.97 (*C*q). FT-IR (KBr, υ_{max}, cm^{-1}): 3600 (adsorbed water), 3030–3090 (sp^2 C-H), 2913 and 2854 (sp^3 C-H), 1930–1780 (overtone of aromatic ring), 1630 (C=C), 1450 (CH_2), 727 and 750 (=C-H) (Figs. S4–S6).

Characterization of C_9H_6-C(4-tBu-cyclo-C_5H_9) (F3)

Fulvene ($C_{19}H_{24}$, F3) was obtained as yellow oil in 75% yield. ^{1}H NMR (400 MHz, $CDCl_3$, δ, ppm): 0.9 (9H, s, C_9H_6-C(4-*t*Bu-*cyclo*-C_5H_9)), 1.4 (3H, m, C_9H_6-C(4-*t*Bu-*cyclo*-C_5H_9)), 2.2 (2H, t, C_9H_6-C(4-*t*Bu-*cyclo*-C_5H_9)), 2.4 (2H, m, C_9H_6-C(4-*t*Bu-*cyclo*-C_5H_9)), 3.2 (1H, d, C_9H_6-C(4-*t*Bu-*cyclo*-C_5H_9)), 3.8 (1H, d, C_9H_6-C(4-*t*Bu-*cyclo*-C_5H_9)), 6.86 (1H, d, C_9H_6-C(4-*t*Bu-*cyclo*-C_5H_9)), 6.96 (1H, d, C_9H_6-C(4-*t*Bu-*cyclo*-C_5H_9)), 7.24-7.30 (2H, m, C_9H_6-C(4-*t*Bu-*cyclo*-C_5H_9)), 7.40 (1H, d, C_9H_6-C(4-*t*Bu-*cyclo*-C_5H_9)), 7.95 (1H, d, C_9H_6-C(4-*t*Bu-*cyclo*-C_5H_9)). ^{13}C NMR (100 MHz, $CDCl_3$, δ, ppm): 27.6 (CH_3), 28.1, 29.3, 31.5, 33.8 (CH_2), 47.5, 121.4, 124, 124.8, 126.1, 127.5, 128.3 (*C*H), 32.8, 133.6, 136, 144.8, 152.1 (C_q). FT-IR (KBr, υ_{max}, cm^{-1}): 3040–3090 (sp^2 C-H), 2870 and 2956 (sp^3 C-H), 1940–1780 (overtone of aromatic ring), 1627 (C=C), 1446 (CH_2), 727 and 748 (=C-H) (Figs. S7–S9).

Characterization of C_9H_6-C(cyclo-C_6H_{12}) (F4)

Fulvene ($C_{16}H_{18}$, F4) was obtained as yellow oil in 75% yield. ^{1}H NMR (400 MHz, $CDCl_3$, δ, ppm): 1.68 (4H, m, C_9H_6-C(*cyclo*-C_6H_{12})), 1.86 (2H, m, C_9H_6-C(*cyclo*-C_6H_{12})), 1.97 (2H, m, C_9H_6-C(*cyclo*-C_6H_{12})), 2.93 (2H, t, C_9H_6-C(*cyclo*-C_6H_{12})), 3.17 (2H, t, C_9H_6-C(*cyclo*-C_6H_{12})), 6.87 (1H, d, C_9H_6-C(*cyclo*-C_6H_{12})), 6.95 (1H, d, C_9H_6-C(*cyclo*-C_6H_{12})), 7.25–7.32 (2H, m, C_9H_6-C(*cyclo*-C_6H_{12})), 7.41 (1H, d, C_9H_6-C(*cyclo*-C_6H_{12})), 7.81 (1H, d, C_9H_6-C(*cyclo*-C_6H_{12})). ^{13}C NMR (100 MHz, $CDCl_3$, δ, ppm): 26.2, 28.6, 28.8, 29.5, 34.5, 34.9 (*C*H_2), 121.2, 123.6, 124.7, 124.9, 126, 127.2 (*C*H), 128.3, 136.1, 144.1, 154 (*C*$_q$). FT-IR (KBr, υ_{max}, cm^{-1}): 3010–3090 (sp^2 C-H), 2852 and 2921 (sp^3 C-H), 1790-1940 (overtone of aromatic ring), 1627 (C=C), 1448 (CH_2), 721 and 750 (=C-H) (Figs. S10–S12).

General procedure for synthesis of ligands [C_9H_6-C(R)]-C_6H_5 (R=cyclo-C_5H_{10} (L1), $(CH_3)_2$ (L2), 4-tBu-cyclo-C_5H_9 (L3), cyclo-C_6H_{12} (L4))

Indenyl-based ligands were prepared according to a slightly modified literature method (Scheme 2) [26]. Solution of synthetic fulvenes derivatives (0.5 mmol) in diethyl ether (3 mL) was added dropwise to the phenyllithium solution in dibuthyl ether (2 mmol, 1.3 mL, 1.9 M) in 5 mL of dry diethyl ether under argon atmosphere at -40 °C. The mixture was stirred at room temperature for 12 h. After one day, the reaction mixture was hydrolyzed by 10 mL of cold water. The aqueous layer was extracted with light petroleum ether (three times), and the organic layer was dried with anhydrous $MgSO_4$. The solvent was removed under vacuum. The obtained L1–L4 ligands were purified using column chromatography via petroleum ether as eluent.

Characterization of [C_9H_7-C(cyclo-C_5H_{10})]-C_6H_5 ligand (L1)

Ligand ($C_{21}H_{22}$, L1) was obtained as a white solid in 91% yield. ^{1}H NMR (400 MHz, $CDCl_3$, δ, ppm): 1.4–1.55 (1H, m, [C_9H_7-C(*cyclo*-C_5H_{10})]-C_6H_5), 1.51–1.66 (5H, m, [C_9H_7-C(*cyclo*-C_5H_{10})]-C_6H_5), 2.23–2.25 (2H, m, [C_9H_7-C(*cyclo*-C_5H_{10})]-C_6H_5), 2.39–2.42 (2H, m, [C_9H_7-C(*cyclo*-C_5H_{10})]-C_6H_5), 3.44 (2H, d, [C_9H_7-C(*cyclo*-C_5H_{10})]-C_6H_5), 6.56 (1H, t, [C_9H_7-C(*cyclo*-C_5H_{10})]-C_6H_5), 7.02–7.1 (3H, m, [C_9H_7-C(*cyclo*-C_5H_{10})]-C_6H_5), 7.15–7.21 (1H, m, [C_9H_7-C(*cyclo*-C_5H_{10})]-C_6H_5), 7.28–7.31 (2H, m, [C_9H_7-C(*cyclo*-C_5H_{10})]-C_6H_5), 7.4–7.49 (3H,

m, [C_9H_7-C(*cyclo*-C_5H_{10})]-C_6H_5). ^{13}C NMR (100 MHz, $CDCl_3$, δ, ppm): 23.03, 26.61, 36.46, 37.48 (CH_2), 44.55 [C_9H_7-*C*(*cyclo*-C_5H_{10})]-C_6H_5, 122.35, 123.64, 123.86, 125.35, 125.67, 127.06, 128.13, 129.61 (*C*H), 143.93, 145.22, 147.38, 149.96 (*C*q). FT-IR (KBr, υ_{max}, cm^{-1}): 2974 (sp^2 C-H), 2933 and 2921 (sp^3 C-H), 1610 (C=C), 1461 ($CH_{2bending}$), 700–800 (=C-H) (Figs. S13–S15).

Characterization of [C_9H_7-$C(CH_3)_2$]-C_6H_5 ligand (L2)

Ligand ($C_{18}H_{18}$, L2) was obtained as a yellow oil in 90% yield. ^{1}H NMR (400 MHz, $CDCl_3$, δ, ppm): 1.75 (6H, s, [C_9H_7-C(*CH*$_3$)$_2$]-C_6H_5), 3.47 (2H, d, [C_9H_7-$C(CH_3)_2$]-C_6H_5), 6.54 (1H, t, [C_9H_7-$C(CH_3)_2$]-C_6H_5), 6.73–6.78 (1H, d, [C_9H_7-$C(CH_3)_2$]-C_6H_5), 7.01–7.08 (1H, t, [C_9H_7-C(CH_3)$_2$]-C_6H_5), 7.10–7.17 (1H, t, [C_9H_7-$C(CH_3)_2$]-C_6H_5), 7.20–7.26 (1H, t, [C_9H_7-$C(CH_3)_2$]-C_6H_5), 7.27–7.34 (2H, t, [C_9H_7-$C(CH_3)_2$]-C_6H_5), 7.35–7.42 (2H, d, [C_9H_7-$C(CH_3)_2$]-C_6H_5), 7.48–7.52 (1H, d, [C_9H_7-C(CH_3)$_2$]-C_6H_5). ^{13}C NMR (100 MHz, $CDCl_3$, δ, ppm): 29.65 (CH_3)$_2$, 37.8 (CH_2), 40.5 [C_9H_7-*C*(CH_3)$_2$]-C_6H_5, 122.34, 123.70, 123.96, 125.47, 125.82, 126.21, 127.42, 128.29 (*C*H), 143.79, 145.28, 148.15, 152.35 (*C*q). FT-IR (KBr, υ_{max}, cm^{-1}): 3072 (sp^2 C-H), 2800–3000 (sp^3 C-H), 1677 (C=C), 1465 ($CH_{2bending}$), 780 (=C-H) (Figs. S16–S18).

*Characterization of [C_9H_7-C(4-tBu-*cyclo*-C_5H_9)]-C_6H_5 ligand (L3)*

Ligand ($C_{25}H_{30}$, L3) was obtained as a white solid in 92% yield. ^{1}H NMR (400 MHz, $CDCl_3$, δ, ppm): 0.8 (9H, s, [C_9H_7-C(4-*t*Bu-*cyclo*-C_5H_9)]-C_6H_5), 1.1–1.2 (1H, m, [C_9H_7-C(4-*t*Bu-*cyclo*-C_5H_9)]-C_6H_5), 1.3–1.53 (2H, m, [C_9H_7-C(4-*t*Bu-*cyclo*-C_5H_9)]-C_6H_5), 1.6–1.80 (2H, t, [C_9H_7-C(4-*t*Bu-*cyclo*-C_5H_9)]-C_6H_5), 1.86–2.07 (2H, t, [C_9H_7-C(4-*t*Bu-*cyclo*-C_5H_9)]-C_6H_5), 2.58–2.85 (2H, m, [C_9H_7-C(4-*t*Bu-*cyclo*-C_5H_9)]-C_6H_5), 3.5 (2H, d, [C_9H_7-C(4-tBu-*cyclo*-C_6H_9)]-C_6H_5)), 6.63–6.79 (1H, t, [C_9H_7-C(4-*t*Bu-*cyclo*-C_5H_9)]-C_6H_5), 6.9–7.2 (4H, m, [C_9H_7-C(4-*t*Bu-*cyclo*-C_6H_9)]-C_6H_5), 7.2–7.34 (2H, m, [C_9H_7-C(4-*t*Bu-*cyclo*-C_6H_9)]-C_6H_5), 7.3-7.5 (3H, m, [C_9H_7-C(4-*t*Bu-*cyclo*-C_5H_9)]-C_6H_5). ^{13}C NMR (100 MHz, $CDCl_3$, δ, ppm): 24.1 (CH_2), 27.5 [C_9H_7-C(4-*t*Bu-*cyclo*-C_5H_9)]-C_6H_5, 32.5, 36.9 (CH_2), 37.7 (CH_2), 44.5, 48 [C_9H_7-*C*(4-*t*Bu-*cyclo*-C_5H_9)]-C_6H_5, 122.5, 123.5, 123.9, 125.3, 125.7, 126.2, 128.2, 131.5 (*C*H), 144.1, 145.1, 147.5, 148.9 (*C*q). FT-IR (KBr, υ_{max}, cm^{-1}): 3010–3085 (sp^2 C-H), 2974 (sp^3 C-H), 1606 (C=C),1458 ($CH_{2bending}$), 700–800 (=C-H) (Figs. S19–S21).

*Characterization of [C_9H_7-C(*cyclo*-C_6H_{12})]-C_6H_5 ligand (L4)*

Ligand ($C_{22}H_{24}$, L4) was obtained as a white solid in 90% yield. ^{1}H NMR (400 MHz, $CDCl_3$, δ, ppm): 1.57–1.92 (8H, m, [C_9H_7-C(*cyclo*-C_6H_{12})]-C_6H_5), 2.24–2.50 (4H, m, [C_9H_7-C(*cyclo*-C_6H_{12})]-C_6H_5), 3.48 (2H, d, [C_9H_7-C(*cyclo*-C_6H_{12})]-C_6H_5), 6.51–6.55 (1H, t, [C_9H_7-C(*cyclo*-C_6H_{12})]-C_6H_5), 6.75–6.79 (1H, d, [C_9H_7-C(*cyclo*-C_6H_{12})]-C_6H_5), 6.98–7.01 (1H, t, [C_9H_7-C(*cyclo*-C_6H_{12})]-C_6H_5), 7.07–7.10 (1H, t, [C_9H_7-C(*cyclo*-C_6H_{12})]-C_6H_5), 7.15–7.19 (1H, t, [C_9H_7-C(*cyclo*-C_6H_{12})]-C_6H_5), 7.25–7.31 (2H, t, [C_9H_7-C(*cyclo*-C_6H_{12})]-C_6H_5), 7.36–7.38 (2H, d, [C_9H_7-C(*cyclo*-C_6H_{12})]-C_6H_5), 7.43–7.54 (1H, d, [C_9H_7-C(*cyclo*-C_6H_{12})]-C_6H_5). ^{13}C NMR (100 MHz, $CDCl_3$, δ, ppm): 24.07, 31.63, 37.36, 39.11 (CH_2), 47.80 [C_9H_7-*C*(*cyclo*-C_6H_{12})]-C_6H_5, 122.5, 123.58, 123.87, 125.37, 125.57, 126.69, 127.49, 128.22 (*C*H), 144.09, 145.27, 148.77, 151.83 (*C*q). FT-IR (KBr, υ_{max}, cm^{-1}): 3025 ($CH_{aromatic,}$ sp^2 C-H), 2971 and 2861 ($CH_{aliphatic,}$ sp^3 C-H), 1610 (C=C), 1467 ($CH_{2bending}$), 792 (=C-H) (Figs. S22–S24).

*Synthesis and characterization of [C_9H_6-C(R)-C_6H_5]$TiCl_3$ complexes with various types of bridges (R=*cyclo*-C_5H_{10} (C1), $(CH_3)_2$ (C2), 4-tBu-*cyclo*-C_5H_9 (C3), and *cyclo*-C_6H_{12} (C4))*

For the synthesis of the desired catalysts, ligands L1–L4 (0.5 mmol) in dry petroleum ether (5 mL), was added dropwise to a solution of the 0.5 mmol n-BuLi (0.2 mL, 2.5 M) solution in petroleum ether at -70 °C under an argon atmosphere. After mixing for four hours at the same temperature, white milky salt was obtained. Then, 0.5 mmol (0.05 mL) of $TiCl_4$ was added to the reaction mixture at -78 °C. As soon as the $TiCl_4$ was added, a dark red solution was obtained. The liver red solution was maintained at room temperature for 12 h. The unreacted solvent and $TiCl_4$ were then removed by vacuum and the residue were dissolved in 10 mL of dry petroleum ether and then centrifuged. After cooling the solution containing the catalyst to -20 °C, the catalysts were obtained (Scheme 2). Catalyst C1 was obtained as dark red crystals in 70% yield. Elemental analysis (%): calculated for $C_{21}H_{21}TiCl_3$ (found): C 58.99 (59.30), H 4.95 (5.12), Ti 11.19 (10.53), Cl 24.87 (—). Catalyst C2 was obtained as dark red solid in 65 % yield. Elemental analysis (%): calculated for $C_{18}H_{17}TiCl_3$ (found): C 55.79 (54.90), H 4.42 (4.40), Ti 12.35 (11.95), Cl 27.44 (—). Catalyst C3 was obtained as dark red solid in 68% yield. Elemental analysis (%): calculated for $C_{25}H_{29}TiCl_3$ (found): C 62.08 (62.22), H 6.04 (6.11), Ti 9.90 (9.12), Cl 21.99 (—). Catalyst C4 was obtained as dark red solid in 73% yield. Elemental analysis (%): calculated for $C_{22}H_{23}TiCl_3$ (found): C 59.83 (59.92), H 5.25 (5.22), Ti 10.84 (9.93), Cl 24.08 (—).

Trimerization of ethylene

The ethylene trimerization reactions were performed using synthetic titanium catalysts in a pressurized steel reactor equipped with a mechanical stirrer. The pressure and temperature inside the reactor and the mixer speed were controlled by the reactor's digital displays. In this regard, the reactor was first purged with dried pure argon at 120 °C for 2 h. It was reached the desired temperature and the solvent and MMAO were injected subsequently. After 10 min, the solution containing catalyst/solvent was injected and trimerization was started by charging the reactor with ethylene monomer. The reaction temperature and ethylene pressure were fixed constant throughout the process. After 30 min, the reactor was cooled to -10 °C. Then, the liquid phase including, 1-C6 and probable by-products were collected and analyzed using GC instrument. The produced polyethylene by-product was also washed with acidified ethanol (3% HCl), and dried under vacuum at 60 °C to a constant weight.

Computational details

DFT static calculations were performed at B3LYP level [46] with the Gaussian16 package [47]. The electronic configuration of the system was described with the standard split valence basis set with a polarization function for all the atoms (def2SVP keyword in Gaussian) of Ahlrichs and co-workers [48]. Geometry optimizations were performed without symmetry constrain, and analytical frequency calculations performed the characterization of the local stationary points. These frequencies were used to calculate unscaled zero-point energies as well as thermal corrections and entropy effects at 298 K and 1 atm. The transition states were located using the synchronous transit-guided quasi-Newton (QST3) approach and the extrema have been checked by analytical frequency calculations. All transition states have associated only one imaginary frequency. Solvent effects were estimated in single point energy calculations on the gas phase optimized structures based on the polarizable continuous solvation model (PCM) [49], as implemented in Gaussian16, using toluene (Tol) as a solvent. Energies were obtained using the B3LYP functional [46], in conjunction with the triple-ζ basis set cc-pVTZ for all the atoms [50], together with the Grimme D3 correction term [51] to the electronic energy. The reported free energies in this work include energies obtained at the B3LYP/cc-pVTZ level of theory corrected with zero-point energies, thermal corrections and entropy effects evaluated at 298 K, achieved at the B3LYP/def2SVP level, without translational entropy corrections [52].

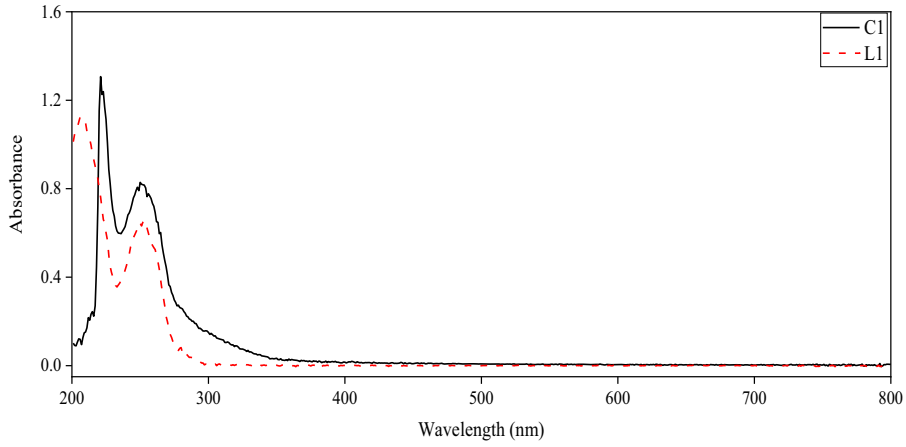

Fig. 1. Comparison between UV–visible absorption spectra of **L1** ligand and corresponding catalyst (**C1**)

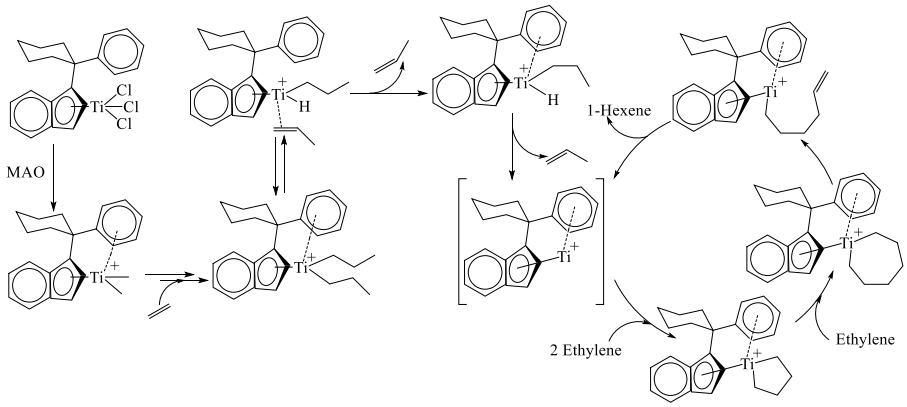

Scheme 3. Proposed mechanism for the key role of MAO in catalyst activation.

Results and discussion

Characterization of catalysts using UV–visible spectroscopy

In the structure of synthetic catalysts, $[C_9H_6\text{-}C(R)\text{-}C_6H_5]TiCl_3$, due to the presence of halide groups and bulky indenyl moiety, the coordination number of Ti is IV [53,54]. In general, for this group of complexes, tetrahedral and square-planar structures are observed. Due to the presence of bulky ligands in the structure and electrostatic repulsion between them, the complex tends to have a deviated tetrahedral structure. For the latter geometry, the steric hindrance has the minimum value [55], and in agreement the relative stability of the complex increases. According to the valence bond theory, orbitals of the valence layer of the central atom in the tetrahedral structure are hybridized either as sp^3 or as d^3s [29]. In our synthesized titanium-based catalysts as well as $TiCl_4$, the electron arrangement of the central atom is d^0. As shown in Fig. 1, due to the d^0 spin of Ti atom in the synthesized catalysts, d→d transitions were not observed for the studied complexes. Actually, the peaks observed at 260–280 nm were related to π→π (intra-ligand) transitions. In addition to this type of transition, the ligand-to-metal transition at about 240 nm was also detected. However, due to the increase in the length of the resonance system, the intra-ligand transition in all catalysts

Table 1
Ethylene trimerization results with C2 catalyst.

Entry	Al/Ti	T (C)	Ethylene pressure (bar)	1-C_6 wt%	1-Hexene (g)	1-Octene (g)	PE (g)	Activity (kg 1-C_6.molTi^{-1}.h^{-1})[a]	Selectivity (wt.% of 1-C6)[b]
1	2000	20	3	1.20	0.208	0.004	0.03	277	85.95
2	2000	20	5	2.46	0.426	0.007	0.14	568	74.34
3	2000	20	8	5.10	0.884	0.011	0.30	1179	73.98
4	2000	20	12	1.46	0.253	0.004	5.60	337	4.32
5	2000	40	8	10.34	1.792	0.040	0.43	2389	79.36
6	2000	60	8	11.22	1.945	0.034	0.49	2593	78.77
7	2000	80	8	2.06	0.357	0.001	0.10	476	77.95
8	2000	40	3	3.91	0.676	0.008	0.10	901	86.22
9	2000	40	5	6.86	1.190	0.017	0.25	1586	81.67
10	2000	40	12	2.01	0.348	0.001	5.70	465	5.76
11	500	40	8	1.80	0.311	0.001	0.003	416	98.73
12	1000	40	8	4.10	0.711	0.001	Trace	948	99.85
13	1500	40	8	9.80	1.699	0.030	0.38	2265	80.56

[a] Time = 30 min, rpm = 1100, solvent = toluene (20 mL).
[b] Percentage of 1-C_6 overall by mass.

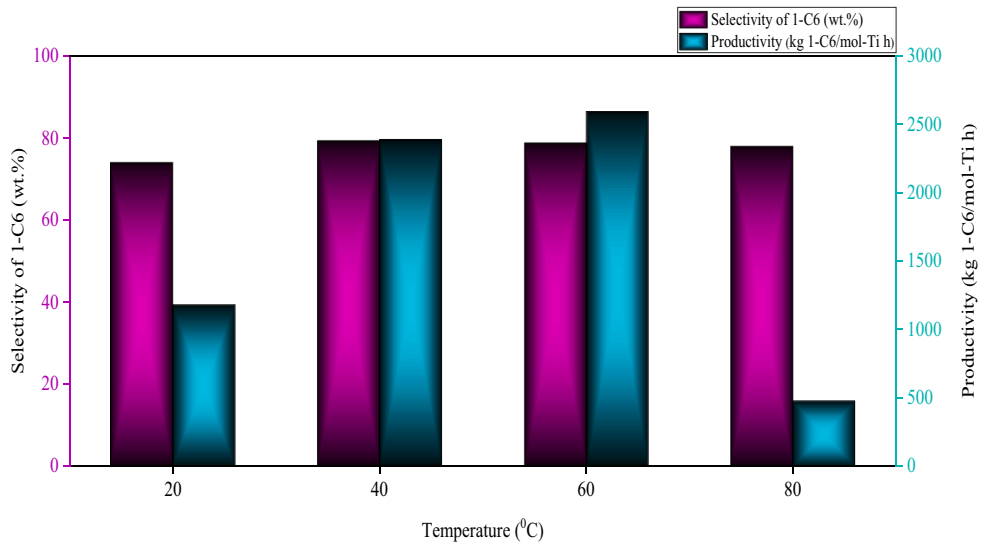

Fig. 2. Effect of reaction temperature on **C2** catalyst productivity; Al/Ti= 2000, time= 30 min, rpm= 600, solvent =toluene (20 mL), catalyst concentration= 1.5 μmol, ethylene pressure= 8 bar.

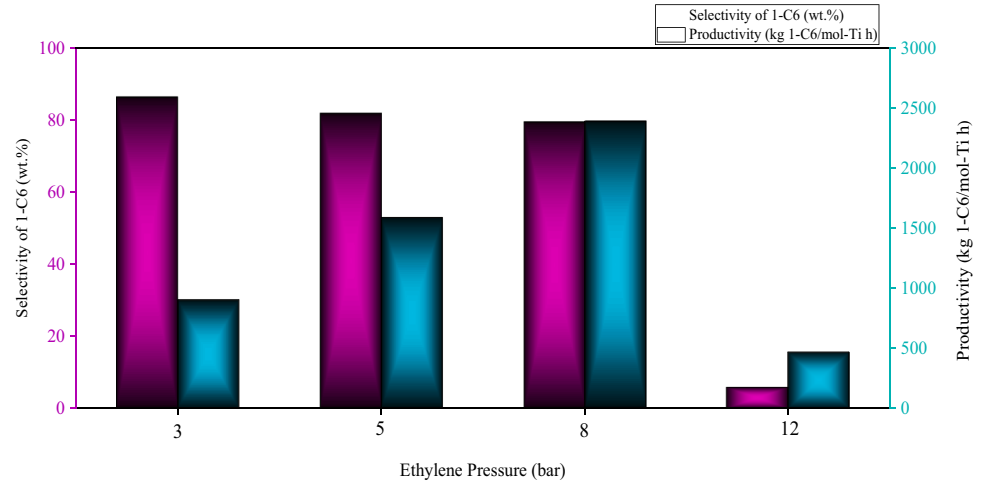

Fig. 3. Effect of ethylene pressure on the catalyst productivity; Al/Ti= 2000, time= 30 min, rpm= 600, solvent = toluene (20 mL), catalyst (**C2**) concentration= 1.5 μmol, temperature= 40 °C.

has shifted to higher wavelengths (Figs. S25–S27).

Ethylene trimerization results using synthesized catalysts (C1–C4)

The ethylene trimerization reaction using the as-synthesized titanium-based catalysts activated by MMAO afforded 1-hexene and some by-products. The key role of co-catalyst, between other functions such as removal of oxygen and water and eliminating environmental pollution, is to reduce the oxidation state of titanium metal and to facilitate the production of cationic species [56]. In general, co-catalyst facilitates alkyl abstraction from the catalyst pioneer to yield an anionic co-catalyst species [RX^-] and a cationic metal species [L_nM^+], which together represent the active catalytic system as an ion pair with [L_nM^+][RX^-] formula (Scheme 3) [54]. The MMAO-activated system was highly active and selective in ethylene trimerization reaction [57]. In fact, an analysis of the liquid fraction by GC disclosed that ethylene trimerization via catalyst/MMAO under different position achieved 1-hexene with high selectivity.

The results of ethylene oligomerization using the C2 catalyst are shown in Table 1. First, the effect of reaction temperature on catalyst activity was investigated (entries 3, 5-7). To do this, the reaction was performed at four temperatures of 20, 40, 60, and 80 °C with 1.5 μmol of C2 catalyst solution, and 8 bar ethylene pressure. From Fig. 2, it is clear that for reaction temperature there is an optimal value of 60 °C, in which catalyst activity and 1-C_6 selectivity have their maximum amount of 2593 kg 1-C_6/mol-Ti h and 78.77%, respectively. It was reported that the pendant ring in the complex structure can coordinate easily to the electron deficient cationic Ti species due to the higher catalyst flexibility at elevated temperatures which subsequently causes a substantial decrease in the catalyst activity [33,58,59].

Due to the negligible productivity difference in the productivity values at the reaction temperatures of 40 °C and 60 °C (2389 and 2593 kg 1-C_6/mol-Ti h, respectively), the temperature of 40 °C was chosen for the next studies. In the next step, effect of ethylene pressure was taken into account. According to Fig. 3, increasing the ethylene pressure from 3 to 8 bar, the activity of the C2 catalyst increased due to the enhanced solubility of ethylene gas at higher pressures. However, after $P = 8$ bar, the reaction switched to ethylene polymerization, so that at $P = 12$ bar, the activity decreased to 337, and 465 kg 1-C_6/mol-Ti h, at the $T = 20$ and 40 °C (entries 4 and 10, Table 1), respectively. Therefore, the next experiments were conducted at $P = 8$ bar as the optimum ethylene pressure value.

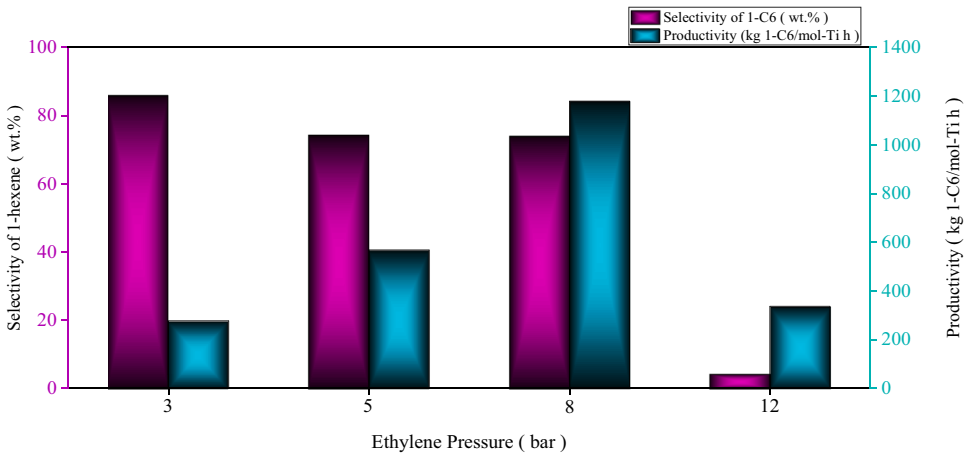

Fig. 4. Effect of ethylene pressure on catalyst productivity; Al/Ti= 2000, time= 30 min, rpm= 600, solvent = toluene (20 mL), catalyst (**C2**) concentration= 1.5 μmol, temperature= 20 °C

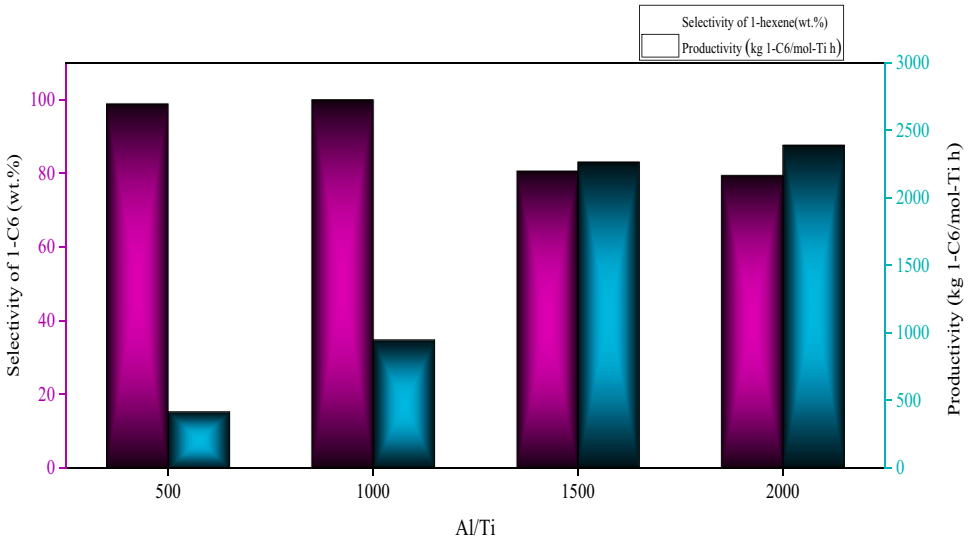

Fig. 5. Effect of ethylene pressure on catalyst productivity; time= 30 min, rpm= 600, solvent= toluene (20 mL) catalyst (C2) concentration= 1.5 μmol, temperature= 40 °C, ethylene pressure= 8 bar

Worth mentioning, effect of ethylene pressure on C2 catalyst activity and 1-C_6 selectivity was considered at T = 20 °C, as well (entries 1–4, Table 1 and Fig. 4). Notably, in this condition the same trend as it at T=40°C was observed. Indeed, the highest catalyst activity and 1-C_6 selectivity of 1179 kg 1-C_6.mol Ti^{-1}.h^{-1} and 74% were obtained at P = 8 bar (entry 3) after which the process was switched to the polymerization reaction with catalyst activity of 1294 kg PE/mol-Ti h.

In the following, effect of Al/Ti molar ratio on the C2 catalyst activity and selectivity was investigated, Fig. 5. Obviously, by increasing Al/Ti molar ratio up to 2000, catalyst activity increases due to the formation of more catalytic active sites. As the Al/Ti ratio raised above 2000, the activity decreased due to the poisoning of catalytic sites. Therefore, Al/Ti=2000 molar ratio was selected as the desired value, due to high activity of C2 catalyst toward 1-C_6 formation.

According to the results, C2, pressure of 8 bar, T = 40 °C and catalyst dosage of 1.5 μmol were selected as the optimum reaction conditions for achieving high catalytic activity and 1-hexene selectivity. Finally, the effect of bridge type on the catalytic efficiency was elucidate. According to the previous studies conducted in these catalyst systems, there is no coordination between dangling arene (phenyl) and Ti metal at the primary precatalyst. However, after activation with the MAO co-catalyst, it happens easily which facilitates the formation of 1-C_6 product [26,60].

Table 2
Ethylene trimerization results with titanium-based catalysts (C1–C4).

Catalyst	Selectivity (wt.% of 1- C_6)[b] with PE	Selectivity (wt.% of 1- C_6) without PE	Activity (kg 1-C_6/mol-Ti h)[a]	PE (g)	1-C_8 (g)	1-C_6 (g)	1-C_6 (wt%)
C1	80.30	98.14	3244	0.55	0.048	2.4328	14.03
C2	79.35	97.76	2389	0.426	0.03	1.792	10.34
C3	77.94	97.85	2129	0.425	0.035	1.5979	9.21
C4	30.25	99.2	989	1.7	0.006	0.7421	4.28

[a] Al/Ti = 2000, time = 30 min, rpm = 600, solvent = toluene (20 mL), catalyst concentration = 1.5 μmol, ethylene pressure =8 bar
[b] Percentage of 1-C6 overall by mass.

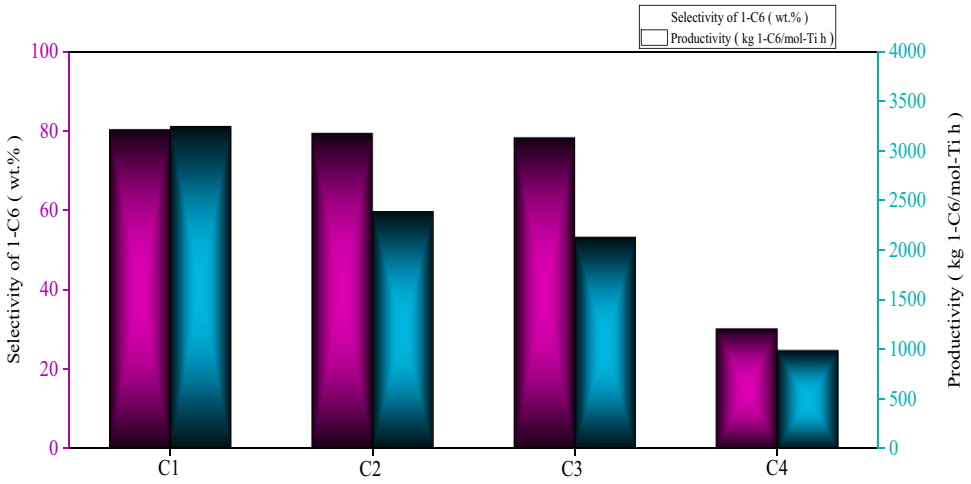

Fig. 6. Effect of various bridges on catalyst productivity; Al/Ti= 2000, time= 30 min, rpm= 600, solvent= toluene (20 mL), catalyst concentration= 1.5 μmol, temperature= 40 °C, ethylene pressure= 8 bar

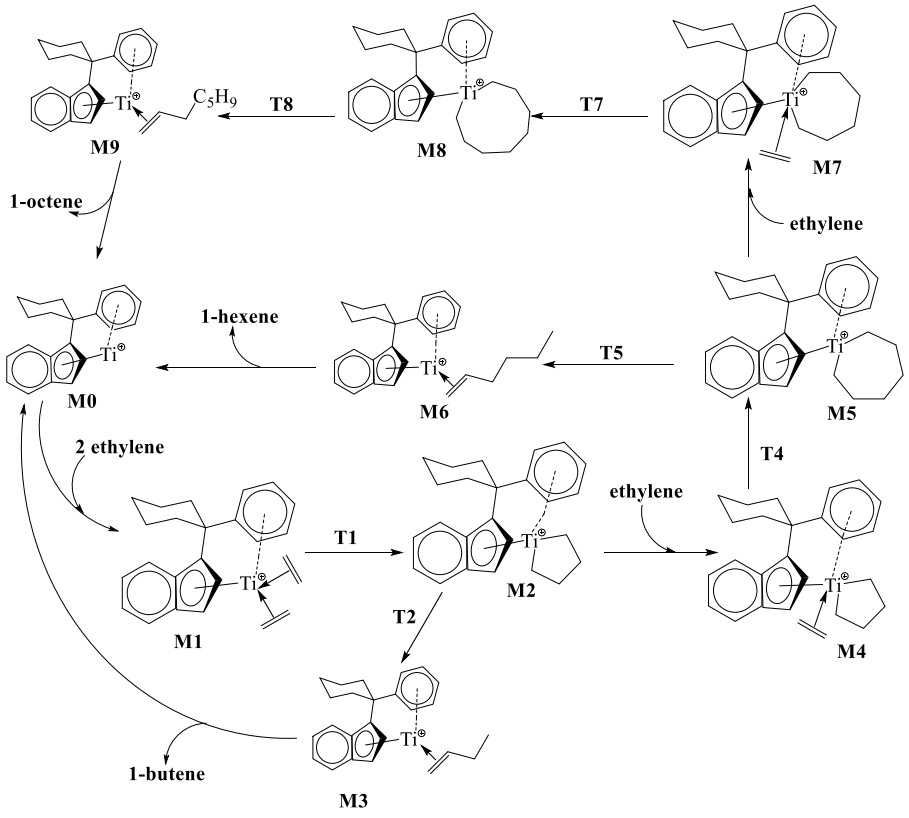

Scheme 4. General mechanism for ethylene trimerization via metallacycle intermediates.

The bridge between the indenyl and phenyl moieties has a significant effect on the direction of phenyl ring relative to the titanium metal center and the size of C(Ind)C(bridge)C(phenyl) angle. When the catalyst is activated by the co-catalyst, the dangling phenyl will go toward the cationic metal with a low oxidation number. Therefore, the type of bridge and its size have a direct effect on the coordination of arene and Ti. In the C1 with the bridge C(*cyclo*-C_5H_{10}), it has stronger coordination than the same complex with the CMe_2 bridge. Catalyst C4 has the most space constraints since the pendant arene moiety has a very strong coordination with Ti. Consequently, this can prevent ethylene from approaching the metal active site. That is, the bridge has a dual effect on catalyst efficiency. While the cycloheptane bridge leads to the largest spatial hindrance and angular pressures, and thus low activity, the catalyst with a cyclohexane bridge with stable chair structure, high activity and selectivity. Table 2 shows the trimerization results for C1–C4 catalysts (see Scheme 1 for the detail of the catalysts).

According to Table 2, it is noteworthy that, regardless of the polymer produced in the trimerization, the selectivity for 1-hexene in all catalysts was higher than 90%. However, considering the unwanted polymer by-product, the selectivity of 1-hexene for all four catalysts decreased. 1-hexene selectivity for catalyst C4 was obtained due to the production of 1.7 g of polyethylene in the reaction of only 30% (Fig. 6).

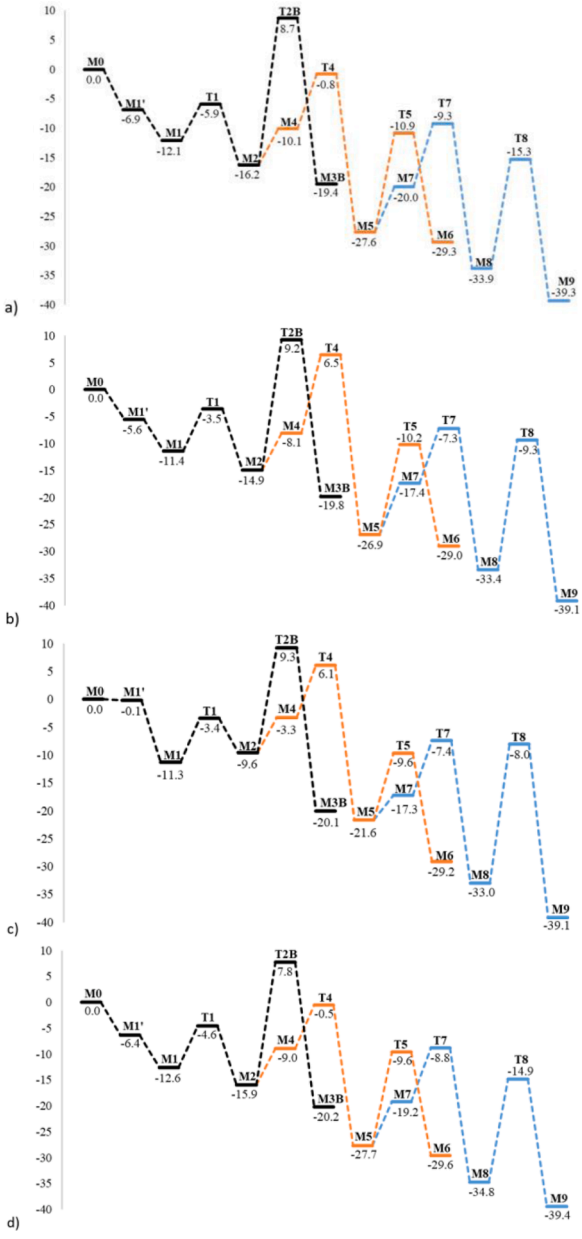

Fig. 7. Gibbs free energy profile (kcal•mol^{-1}) for the ethylene oligomerization by catalysts (a) C1, (b) C2, (c) C3 and (d) C4, relative to compound M0 and considering toluene as a solvent.

Evaluation of ethylene oligomerization reaction using as-synthesized half-sandwich titanium-based catalysts by applying density functional theory (DFT)

In the last part of our study, to compare quantitatively the effect of ligand type on the energy values of ethylene trimerization reaction path, and shed light on the structural parameters, DFT calculations were carried out. In this regard, the main responsible and effective steps in the reaction pathways were considered (Scheme 4).

The catalyst activation steps by the MAO co-catalyst (Scheme 3) were not considered and M0 is our starting active catalyst (see Scheme 4), in which the titanium has an oxidation state II. Thus, it has a severe electron deficiency and tends to coordinate rapidly with the two ethylene molecules leading to M1 (note that in the energy profile the insertion of only one ethylene molecule (M1') has also been considered) [61], from which a five-membered metallacycle is formed (M2), switching the corresponding oxidation of the metal center from Ti(II) to Ti(IV). It is possible that as a result of the ring-opening reaction 1-butene will be formed through two different reaction pathways. The first mechanism is the β-hydrogen transfer to Ti, forming a hydride, and the subsequent elimination, the second mechanism is the transfer of intramolecular β-hydrogen and the formation of M3, which means a reduction of the metal center again to Ti(II), and the olefin is bonded to titanium. Since 1-butene is not formed, instead the reaction will lead to the formation of M4 and the third ethylene molecule will be coordinated. After ethylene insertion (M5), the reaction likely continues with a ring-opening (M6) to finally produce 1-C_6 (experimentally observed). However, a new ethylene molecule may bond to titanium and M7 may be formed, leading to the release of 1-octene or even higher olefins such as 1-decene. However, the latter species was not observed experimentally. After considering the general path shown in Scheme 4, the structure of the catalysts was optimized. Since 1-hexene was observed experimentally as the main product and 1-octene as the by-product, only the energy of these steps was investigated for the four catalysts included in Fig. 5. The energy diagram for ethylene oligomerization was then obtained for the four catalysts. In summary, the catalysts can evolve via four main stages of release of 1-butene, the formation of a seven-membered ring, the release of 1-hexene, and the formation of a nine-membered ring.

The reaction mechanism proposed in Scheme 4 has been studied for the four different catalysts C1–C4. In general, results in Fig. 7 are similar for the different candidates. In all cases, the formation of the seven-membered metallacycle (M5) through an insertion of a third molecule of ethylene (T4) is more kinetically favorable than the release of a 1-butene molecule through the intramolecular β-hydride transfer (T2B). This difference is more significant in systems C2 (9.5 kcal•mol^{-1}) and C4 (8.3 kcal•mol^{-1}) than in systems C1 (2.7 kcal•mol^{-1}) and C3 (3.2 kcal•mol^{-1}). These observations match with the experimental evidence reported above, since it has not been observed any release of 1-butene molecules. After the formation of the seven-membered ring (M5) the mechanism proposes both the insertion of a fourth ethylene molecule subsequently forming a nine-membered metallacycle (M8) or, the release of a 1-hexane molecule through, again, an intramolecular β-hydride elimination, leading to M6, being the latter, the winner not thermodynamically, but kinetically speaking. The transition state involving the intramolecular migration of the β-hydrogen (T5) (see Fig. 8a) is thus lower in energy than the transition state involving the formation of the nine-membered metallacycle (T7) (see Fig. 8b). Matter of fact, in all cases the expected product is the 1-hexene while 1-octane becomes only a by-product. The catalysts showing better selectivity towards 1-hexene release is the system C1 as the difference in energy is around 2.9 kcal•mol^{-1}, being C4 the one showing less selectivity as this difference is only 0.8 kcal•mol^{-1}, with C2 and C3 in between, with values of 1.6 and 2.2 kcal•mol^{-1}, respectively. Again, these observations match with the experimental data reported before.

According to the summarized data included in Table 3 (all the optimized geometries and more relevant distances are collected in Table S1 in the supporting information), the energy barrier of ΔE_{TS} for the formation of the seven-membered ring is lower than for the release of 1-butene. On the other hand, the energy barrier of ΔE_{TS} to release 1-hexene is lower than for the formation of a nine-membered ring. Because the amount of ΔE_2 is less than that of ΔE_1, the reaction tends to form 1-hexene. Calculations for other catalysts are shown in Table 3, indicating that the most feasible path is the formation of 1-hexene. The C4 catalyst has a lower selectivity than other catalysts. Anyway, still the next kinetic barrier leading to M9 is higher, and thus the 1-octene formation is even more disfavored than the 1-hexene one, for the four catalysts C1-C4.

To evaluate the sterics among the series C1–C4 the $\%V_{Bur}$ of the rate determining intermediate M5 was evaluated [62,63]. The values are 26.9, 25.4, 27.0 and 26.3%, respectively. Even though the cyclohexane based systems C1 and C3 have a more hindered metal center [64], the difference is scarce and not enough to describe any trend (see Tables S28–S31 for further details) [65–67]. Nor can emphasis be placed on weak interactions such as non-covalent ones [68], since for the four

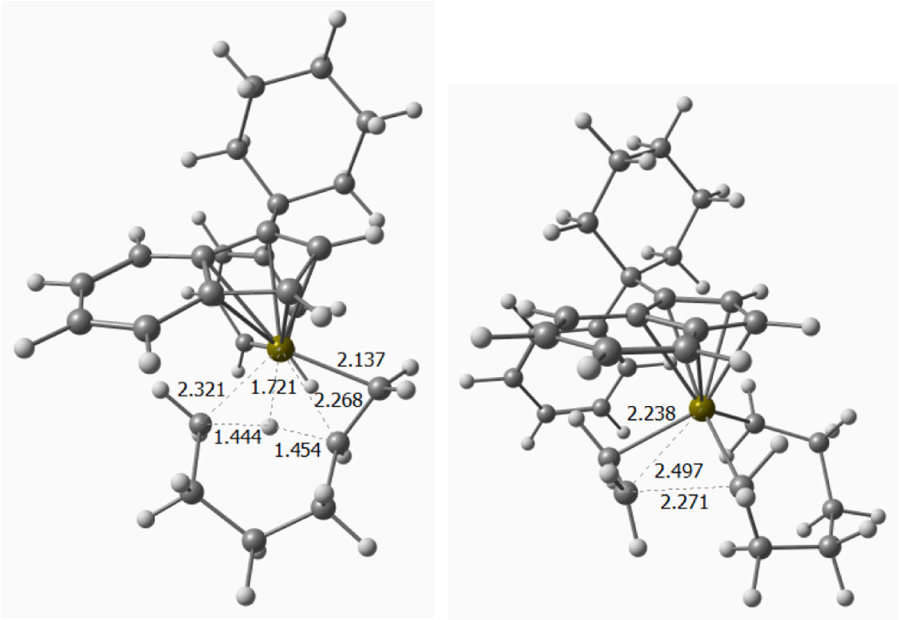

Fig. 8. Optimized geometries for the transition states T5 (a) and T7 (b) for catalyst C1 (main distances in Å).

Table 3
Summary of relative energies (in kcal•mol^{-1}) obtained for different stages of ethylene oligomerization by C1-C4 titanium-based catalysts.

Catalyst name	C1	C2	C3	C4
1-Bu release	24.1	24.9	18.9	23.7
C_7 ring formation	21.4	15.4	15.7	15.4
ΔE_1	2.7	9.5	3.2	8.3
1-Hex release	16.7	16.7	12.0	18.1
C_9 ring formation	19.6	18.3	14.2	18.9
ΔE_2	2.9	1.6	2.2	0.8
1-Oct release	24.1	18.6	25.0	19.9

catalysts the H-bonds are almost identical.

Conclusions

High selectivity and productivity of 1-hexene production was obtained using the four titanium-based catalysts C1–C4, in good comparison with recent work [69]. Ethylene trimerization was performed using these synthetic catalysts with changes in MAO concentration, reaction temperature, and ethylene pressure. Using the C2 catalyst, the concentration of 1.5 μm for the C2 catalyst, the selectivity, and activity of the three catalysts C1, C3, and C4 were also examined in this optimal concentration. The activity of all four catalysts increased with increasing temperature to 60 °C, indicating the thermal resistance of synthetic catalysts at high temperatures. Increasing ethylene pressure always increases the solubility of ethylene and increases the activity, which was also true for the synthesized titanium-based catalysts but, the C2 catalyst moves from ethylene trimerization to ethylene polymerization at an ethylene pressure of 12 bar at 20 and 40 °C.

Declaration of Competing Interest

The authors state that “There are no conflicts to declare”.

Acknowledgments

This work was supported by the Iran National Science Foundation (INSF) through the grant number of 98020308. A.P. is a Serra Húnter Fellow and ICREA Academia Prize 2019, and thanks the Spanish MINECO for project PGC2018-097722-B-I00 and CTQ2017-85341-P. G. P. gratefully acknowledges the support of Institut de Química Computacional i Catàlisi (IQCC) and the computer resources and technical support provided by the Barcelona Supercomputing Center (BSC).

Supplementary materials

Supplementary material associated with this article can be found, in the online version, at doi:10.1016/j.mcat.2021.111636.

References

[1] Y.K. Kim, J. Park, S. Yoon, S.B. Park, Selective ethylene trimerization with a cyclopentadienyl-arene titanatrane catalyst, Transit. Met. Chem. 37 (2012) 439–444.
[2] A. Hanifpour, N. Bahri-Laleh, M. Nekoomanesh-Haghighi, A. Poater, Coordinative chain transfer polymerization of 1-decene in the presence of a Ti-based diamine bis (phenolate) catalyst: a sustainable approach to produce low viscosity PAOs, Green Chem. 22 (2020) 4617–4626.
[3] Y.V. Kissin, Oligomerization reactions of 1-hexene with metallocene catalysts: detailed data on reaction chemistry and kinetics, Mol. Catal. 463 (2019) 87–93.
[4] J. Skupinska, Oligomerization of a-olefins to higher oligomers, Chem. Rev. 91 (1991) 613–648.
[5] R. Sun, L. Liu, R.H. Cheng, Z. Liu, B.P. Liu, Effects of ether electron donors on Cr/PNP-catalyzed ethylene selective oligomerization, J. Mol. Catal. 33 (2019) 103–112.
[6] A. Hanifpour, N. Bahri-Laleh, M. Nekoomanesh-Haghighi, A. Poater, Group IV diamine bis(phenolate) catalysts for 1-decene oligomerization, Mol. Catal. 493 (2020), 111047.
[7] D.P. Solowey, M.V. Mane, T. Kurogi, P.J. Carroll, B.C. Manor, M.H. Baik, D. J. Mindiola, A new and selective cycle for dehydrogenation of linear and cyclic alkanes under mild conditions using a base metal, Nat. Chem. 9 (2017) 1126–1137.
[8] J. Ferreira, R. Zilz, I.S. Boeira, S.M. da Silva, A.C. Casagrande, O.L. Casagrande, Chromium complexes based on thiophene–imine ligands for ethylene oligomerization, Appl. Organomet. Chem. 33 (2019) e4697.
[9] V.C. Gibson, S.K. Spitzmesser, Advances in non-metallocene olefin polymerization catalysis, Chem. Rev. 103 (2003) 283–315.
[10] D.S. McGuinness, Olefin oligomerization via metallacycles: dimerization, trimerization, tetramerization, and beyond, Chem. Rev. 111 (2011) 2321–2341.

[11] R.A. Hackler, G. Kang, G.C. Schatz, P.C. Stair, R.P. Van Duyne, Analysis of TiO_2 atomic layer deposition surface chemistry and evidence of propene oligomerization using surface-enhanced raman spectroscopy, J. Am. Chem. Soc. 141 (2018) 414–422.

[12] M. Rouen, P. Queval, E. Borré, L. Falivene, A. Poater, M. Berthod, F. Hugues, L. Cavallo, O. Baslé, H. Olivier-Bourbigou, M. Mauduit, Selective metathesis of α-Olefins from bio-sourced fischer–tropsch feeds, ACS Catal. 6 (2016) 7970–7976.

[13] I.A. Hussein, T. Hameed, B.F.A. Sharkh, K. Mezghani, Miscibility of hexene-LLDPE and LDPE blends: influence of branch content and composition distribution, Polymer 44 (2003) 4665–4672.

[14] I.A. Hussein, T. Hameed, Influence of branching characteristics on thermal and mechanical properties of Ziegler–Natta and metallocene hexene linear low-density polyethylene blends with low-density polyethylene, J. Appl. Polym. Sci. 97 (2005) 2488–2498.

[15] C. Bariashir, C. Huang, G.A. Solan, W.H. Sun, Recent advances in homogeneous chromium catalyst design for ethylene tri-, tetra-, oligo- and polymerization, Coord. Chem. Rev. 385 (2019) 208–229.

[16] C. Wang, J.L. Huang, Catalytic trimerization of ethylene with highly active half-sandwich titanium complexes bearing pendant *p*-fluorophenyl groups, Chin. J. Chem. 24 (2006) 1397–1401.

[17] M. Soheili, Z. Mohamadnia, B. Karimi, Switching from ethylene trimerization to ethylene polymerization by chromium catalysts bearing sns tridentate ligands: process optimization using response surface methodology, Catal. Lett. 148 (2018) 3685–3700.

[18] D.S. McGuinness, P. Wasserscheid, W. Keim, C. Hu, U. Englert, J.T. Dixon, C. Grove, Novel Cr-PNP complexes as catalysts for the trimerisation of ethylene, Chem. Commun. (2003) 334–335.

[19] D.S. McGuinness, P. Wasserscheid, W. Keim, D. Morgan, J.T. Dixon, A. Bollmann, H. Maumela, F. Hess, U. Englert, First Cr(III)−SNS complexes and their use as highly efficient catalysts for the trimerization of ethylene to 1-hexene, J. Am. Chem. Soc. 125 (2003) 5272–5273.

[20] M. Fallahi, E. Ahmadi, A. Ramazani, Z. Mohamadnia, Trimerization of ethylene catalyzed by Cr-based catalyst immobilized on the supported ionic liquid phase, J. Organomet. Chem. 848 (2017) 149–158.

[21] M. Marefat, E. Ahmadi, Z. Mohamadnia, Influence of ionic liquid counterions on activity and selectivity of ethylene trimerization using chromium-based catalysts in biphasic media, Appl. Organomet. Chem. 34 (2020) e5874.

[22] R. Arteaga-Müller, H. Tsurugi, T. Saito, M. Yanagawa, S. Oda, K. Mashima, New tantalum ligand-free catalyst system for highly selective trimerization of ethylene affording 1-hexene: new evidence of a metallacycle mechanism, J. Am. Chem. Soc. 131 (2009) 5370–5371.

[23] M. Fallahi, E. Ahmadi, Z. Mohamadnia, Effect of inorganic oxide supports on the activity of chromium-based catalysts in ethylene trimerization, Appl. Organomet. Chem. 33 (2019) e4975.

[24] E. Naji-Rad, M. Gimferrer, N. Bahri-Laleh, M. Nekoomanesh-Haghighi, R. Jamjah, A. Poater, Exploring basic components effect on the catalytic efficiency of chevron-phillips catalyst in ethylene trimerization, Catalysts 8 (2018) 224.

[25] R.M. Manyik, W.E. Walker, T.P. Wilson, A soluble chromium-based catalyst for ethylene trimerization and polymerization, J. Catal. 47 (1977) 197–209.

[26] Y. Zhang, C. Wang, T. Wu, M.J. Huang, Highly selective trimerization of ethylene with half-sandwich cyclopentadienyl and indenyl titanium complexes bearing pendant thienyl group, J. Mol. Catal. A Chem. 387 (2014) 20–30.

[27] E. Ahmadi, Z. Mohamadnia, M.N. Haghighi, High productive ethylene trimerization catalyst based on $CrCl_3$/SNS ligands, Catal. Lett. 141 (2011) 1191–1198.

[28] P.J. Deckers, B. Hessen, J.H. Teuben, Switching a catalyst system from ethene polymerization to ethene trimerization with a hemilabile ancillary ligand, Angew. Chem. Int. Ed. 40 (2001) 2516–2519.

[29] A. Bollmann, K. Blann, J.T. Dixon, F.M. Hess, E. Killian, H. Maumela, D. S. McGuinness, D.H. Morgan, A. Neveling, S. Otto, M. Overett, Ethylene tetramerization: a new route to produce 1-octene in exceptionally high selectivities, J. Am. Chem. Soc. 126 (2004) 14712–14713.

[30] L. Azimnavahsi, Z. Mohamadnia, Optimization of ethylene trimerization using catalysts based on $TiCl_3$/half-sandwich ligands, Appl. Organomet. Chem. 33 (2019) e4666.

[31] L. Chen, G. Li, Z. Wang, S. Li, M. Zhang, X. Li, Ethylene oligomerization over nickel supported silica-alumina catalysts with high selectivity for C_{10+} products, Catalysts 10 (2020) 180.

[32] P.J.W. Deckers, B. Hessen, J.H. Teuben, Switching a catalyst system from ethene polymerization to ethene trimerization with a hemilabile ancillary ligand, Angew. Chem. Int. Ed. 40 (2001) 2516–2519.

[33] P.J.W. Deckers, B. Hessen, J.H. Teuben, Catalytic trimerization of ethene with highly active cyclopentadienyl-arene titanium catalysts, Organometallics 21 (2002) 5122–5135.

[34] E. Otten, A.A. Batinas, A. Meetsma, B. Hessen, Versatile coordination of cyclopentadienyl-arene ligands and its role in titanium-catalyzed ethylene trimerization, J. Am. Chem. Soc. 131 (2009) 5298–5312.

[35] J. Huang, T. Wu, Y. Qian, Ethylene trimerization with a half-sandwich titanium complex bearing a pendant thienyl group, Chem. Commun. 22 (2003) 2816–2817.

[36] T. Wu, Y. Qian, J. Huang, Hydrogenation of fast pyrolyis oil and model compounds in a two-phase aqueous organic system using homogeneous ruthenium catalysts, J. Mol. Catal. A Chem. 214 (2004) 227–236.

[37] Y. Zhang, H. Ma, J. Huang, Highly selective ethylene trimerization catalyzed by half-sandwich indenyl titanium complexes with pendant arene groups and MAO, J. Mol. Catal. A Chem. 373 (2013) 85–95.

[38] N. Bahri-Laleh, A. Hanifpour, S.A. Mirmohammadi, A. Poater, M. Nekoomanesh-Haghighi, G. Talarico, L. Cavallo, Computational modeling of heterogeneous Ziegler-Natta catalysts for olefins polymerization, Interaction of common cocatalysts in Ziegler-Natta catalyzed olefin, Prog. Polym. Sci. 84 (2018) 89–114.

[39] M. Fallah, N. Bahri-Laleh, K. Didehban, A. Poater, Interaction of common cocatalysts in Ziegler-Natta catalyzed olefin polymerization, Appl. Organomet. Chem. 34 (2020) e5333.

[40] V. Varga, T. Hodík, M. Lamač, M. Horáček, A. Zukal, N. Žilková, W.O. Parker, J. Pinkas, Homogeneous and heterogeneous cyclopentadienyl-arene titanium catalysts for selective ethylene trimerization to 1-hexene, J. Organomet. Chem. 777 (2015) 57–66.

[41] F.F. Karbach, J.R. Severn, R. Duchateau, Effect of aluminum alkyls on a homogeneous and silica-supported phenoxy-imine titanium catalyst for ethylene trimerization, ACS Catal. 5 (2015) 5068–5076.

[42] A. Hanifpour, N. Bahri-Laleh, M. Nekoomanesh-Haghighi, A. Poater, 1-Decene oligomerization by new complexes bearing diamine-diphenolates ligands: effect of ligand structure, Appl. Organomet. Chem. 35 (2021) e6227.

[43] A. Jalali, M. Nekoomanesh-Haghighi, S. Dehghani, N. Bahri-Laleh, Group IV diamine bis(phenolate) catalysts for 1-decene oligomerization, Appl. Organomet. Chem. 34 (2020) e5338.

[44] R. Lapenta, A. Buonerba, E. Luciano, F.D Monica, A. De Nisi, M. Monari, A. Grassi, C. Capacchione, S. Milione, Phenylene-bridged OSSO-type titanium complexes in the polymerization of ethylene and propylene, ACS Omega 3 (2018) 11608–11616.

[45] K.J. Stone, R.D. Little, An exceptionally simple and efficient method for the preparation of a wide variety of fulvenes, J. Org. Chem. 49 (1984) 1849–1853.

[46] P.J. Stephens, F.J. Devlin, C.F. Chabalowski, M.J. Frisch, Ab Initio Calculation of Vibrational Absorption and Circular Dichroism Spectra Using Density Functional Force Fields, J. Phys. Chem. 98 (1994) 11623.

[47] M.J. Frisch, G.W. Trucks, H.B. Schlegel, et al., Gaussian 16, Revision C.01, Gaussian, Inc., Wallingford CT, 2016.

[48] A. Schäfer, H. Horn, R. Ahlrichs, Fully optimized contracted Gaussian basis sets for atoms Li to Kr, J. Chem. Phys. 97 (1992) 2571–2577.

[49] V. Barone, M. Cossi, Quantum calculation of molecular energies and energy gradients in solution by a conductor solvent model, J. Phys. Chem. A 102 (1998) 1995–2001.

[50] R.A. Kendall, T.H. Dunning, R.J. Harrison, Electron affinities of the first-row atoms revisited. Systematic basis sets and wave functions, J. Chem. Phys. 96 (1992) 6796.

[51] S. Grimme, J. Antony, S. Ehrlich, H. Krieg, A consistent and accurate ab initio parametrization of density functional dispersion correction (DFT-D) for the 94 elements H-Pu, Chem. Phys. 132 (2010), 154104.

[52] L. Falivene, G. Talarico, V. Barone, Unraveling the role of entropy in tuning unimolecular vs. bimolecular reaction rates: the case of olefin polymerization catalyzed by transition metals, Mol. Catal. 452 (2018) 138–144.

[53] I. Saeed, S. Katao, K. Nomura, Synthesis and structural analysis of (Cyclopentadienyl)(pyrrolide)titanium(IV) complexes and their use in catalysis for olefin polymerization, Organometallics 28 (2009) 111–122.

[54] R. Bína, I. Císařová, M. Pavlišta, I. Pavlík, Crystallographic report: the [bis(η^5-cyclopentadienyl)titanium(IV)-bis(L-methionine)] dichloride, Appl. Organomet. Chem. 18 (2004) 262–263.

[55] L. Falivene, Z. Cao, A. Petta, L. Serra, A. Poater, R. Oliva, V. Scarano, L. Cavallo, Towards the online computer-aided design of catalytic pockets, Nat. Chem. 11 (2019) 872–879.

[56] W.J. van Rensburg, J.A. van den Berg, P.J. Steynberg, Role of MAO in Chromium-Catalyzed Ethylene Tri- and Tetramerization: a DFT study, Organometallics 26 (2007) 1000–1013.

[57] A.N.J. Blok, P.H.M. Budzelaar, A.W. Gal, Mechanism of ethene trimerization at an ansa-(Arene)(cyclopentadienyl) titanium fragment, Organometallics 22 (2003) 2564–2570.

[58] P. Foster, J.C. Chien, M.D. Rausch, Highly stable catalysts for the stereospecific polymerization of styrene, Organometallics 15 (1996) 2404–2409.

[59] J.C. Flores, J.S. Wood, J.C. Chien, M.D. Rausch, [1-(2-Phenylethyl)-2,3,4,5-tetramethylcyclopentadienyl]- titanium compounds. synthesis and their use for the syndiospecific polymerization of styrene, Organometallics 15 (1996) 4944–4950.

[60] P.R. Elowe, C. McCann, P.G. Pringle, S.K. Spitzmesser, J.E. Bercaw, Nitrogen-linked diphosphine ligands with ethers attached to nitrogen for chromium-catalyzed ethylene tri- and tetramerizations, Organometallics 25 (2006) 5255–5260.

[61] A. Saidi, M.K. Samantaray, A. Poater, M. Tretiakov, L. Cavallo, J.M. Basset, Metathesis of classical and functionalized olefins catalyzed by silica-supported single-site well-defined W and MO pre-catalysts, ChemCatChem 12 (2020) 6067–6075.

[62] A. Poater, B. Cosenza, A. Correa, S. Giudice, F. Ragone, V. Scarano, L. Cavallo, SambVca: a web application for the calculation of buried volumes of N-heterocyclic carbene ligands, Eur. J. Inorg. Chem. (2009) 1759–1766.

[63] L. Falivene, R. Credendino, A. Poater, A. Petta, L. Serra, R. Oliva, V. Scarano, L. Cavallo, SambVca 2. A web tool for analyzing catalytic pockets with topographic steric maps, Organometallics 35 (2016) 2286–2293.

[64] J.A. Luque-Urrutia, A. Poater, The fundamental noninnocent role of water for the hydrogenation of nitrous oxide by PNP pincer RU-based catalysts, Inorg. Chem. 56 (2017) 14383–14387.

[65] J. Poater, M. Gimferrer, A. Poater, Covalent and ionic capacity of MOFs to sorb small gas molecules, Inorg. Chem. 57 (2018) 6981–6990.

[66] L. Falivene, L. Cavallo, G. Talarico, Buried volume analysis for propene polymerization catalysis promoted by group 4 metals: a tool for molecular mass prediction, ACS Catal. 5 (2015) 6815–6822.

[67] A. Poater, L. Cavallo, Comparing families of olefin polymerization precatalysts using the percentage of buried volume, Dalton Trans. (2009) 8878–8883.
[68] L. Falivene, L. Cavallo, G. Talarico, The role of noncovalent interactions in olefin polymerization catalysis: a further look to the fluorinated ligand effect, Mol. Catal. 494 (2020), 111118.
[69] A. Cordier, P.A. Breuil, T. Michel, L. Magna, H. Olivier-Bourbigou, J. Raynaud, C. Boisson, V. Monteil, Titanium-based phenoxy-imine catalyst for selective ethylene trimerization: effect of temperature on the activity, selectivity and properties of polymeric side products, Catal. Sci. Technol. 10 (2020) 1602–1608.